Pyroclastic material on Aristarchus Plateau is tens of meters thick (McEwen et al., 1994), thicker than the regolith layer responsible for equilibration of roughness; if the mechanical properties of the regolith forming from the pyroclasic material differ significantly from the typical maria and highlands, this could explain the observed contrast. The second and third largest pyroclastic deposits in Sinus Aestuum (Gaddis et al., 2003) are rather smooth at the roughness map scale, but do not look like distinctive units.

As we already noted in Section 3, roughness variations over typical terrains, unrelated to impacts, are rather small. The roughness of maria varies over the 0.7–1.1 range, with one exception, mare infill of Tsiolkovsky basin, which is unusually rough ($r \approx 1.4$). The roughness of cratered highlands varies from 0.9 to 1.3. These variations seem regional: a vast region in the north-eastern-central farside is generally rough, even if we consider surfaces between rougher rays of Jackson and Ohm, and a vast region of the southern farside (similar to the extent of South Pole-Aitken basin, SPA) is generally smooth.

Fig. 12 provides a global view of hectometer-scale roughness variations over the Moon by presenting the roughness map (Figs. 2 and 3) smoothed down to the lowest spherical harmonics. It is seen that at the global scale, the tropics are generally rougher than the poles, and the eastern-central farside is a prominent global roughness maximum. Dynamic considerations and modeling (Morota et al., 2008; Gallant et al., 2009; Ito and Malhotra, 2010; Le Feuvre and Wieczorek, 2011) predicted somewhat higher (tens of percents) effective impact crater formation rates in the tropics than at the poles, and somewhat higher rates at the apex (the center of western hemisphere) than at antapex. The observed global roughness pattern correlates with this predicted cratering rate distribution (although the roughness maximum is shifted westward from the apex). This correlation can be causal: since the equilibrated roughness results from a balance between roughening by hectometer-scale impacts and smoothing by regolith gardening, the higher impact rate may shift the equilibrium toward a higher roughness. This explanation is based on the plausible assumption that the projectiles forming hectometer-scale craters are distributed similarly to the observed larger near-Earth asteroids, while the micrometeorites comprise a different, more isotropic population.

It is seen (Fig. 12) that the global distribution of hectometer-scale roughness correlates well with global topography. The correlation coefficient between roughness and topography for spherical harmonics of degree 2 is 0.94 and is statistically significant (the random occurrence of this high correlation is formally excluded with 99.5% confidence). For degrees 3 and 4 the correlation is also rather high (0.79 and 0.78) and marginally significant (98% and 99%). On the basis of geodynamical reasoning, the equator is close to the topographic highs, and relative roughening of the equatorial region might be caused by more frequent impacts, as discussed above. This explains high values of $C_{2,0}$ spherical harmonic for both topography and roughness and thus explains some part of the observed correlation. The similarity between other global-scale details of the distributions is difficult to explain; in principal, it might be coincidental. A possible causal explanation could be related, for example, to levitating dust (e.g., Colwell et al., 2007): the dust might tend to migrate toward lower gravitational potential, which might lead to a global topographic trend of regolith mechanical properties, which in turn could cause a dependence of roughness on elevation.

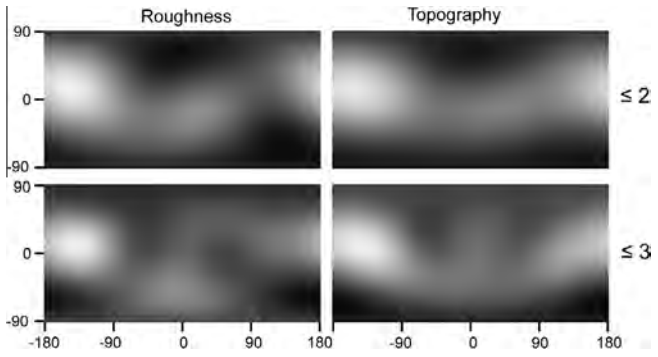

Fig. 12. Global maps of roughness at 115 m baseline and topography smoothed down to spherical harmonics of degree ⩽2 and ⩽3. Simple cylindrical projection. Brighter shades denote higher roughness and higher elevations with respect to a sphere.

5. Kilometer-scale roughness

5.1. Impact craters and basins

After the mare–highland dichotomy, discussed in Section 3, the most prominent feature of the kilometer-scale roughness maps (Figs. 1, 4, and 5) is the Orientale impact basin (Head, 1974; Head et al., 1993, 2010a). The Orientale basin is seen in the roughness maps as a rough ring comprised of the Outer Montes Rook (the middle of the three rings forming the multi-ring basin), a rough annulus composed of the Hevelius Formation (Orientale basin ejecta) outside Montes Cordillera (the outermost topographic ring) and a set of rough radial rays. The prominent individual rays correspond to chains of large secondary craters well seen in the images (e.g., chapter by McCauley in Wilhelms (1987)).

Other large impact basins do not have a similar roughness expression. Kreslavsky and Head (2012) argued that the difference in exposure to the impactor flux between Orientale, the youngest basin of its size, and other basins, such as Imbrium, is too small to account for the observed difference in the roughness signature. They suggest that basin-forming impacts resurface and smooth the kilometer-scale relief globally due to seismic effects, which occur before the rougher ejecta are emplaced. In this way each basin-forming impact erases kilometer-scale roughness signature of all preceding basins, leaving only the last one. If this hypothesis is correct, all distinctively rough features (at kilometer scales) should postdate the Orientale impact; in other words, they could be of Copernican, Eratosthenian or Late Imbrian age, but not older.

More subdued crater-related features are also observed in the kilometer-scale roughness data in the Orientale region at these scales, despite the superposed ejecta and distal smoothing associated with the Orientale seismic effects (e.g., Kreslavsky and Head, 2012). Fassett et al. (2011) used the identification of pre-Orientale craters and assessment of the level of filling to quantify the thickness of Orientale ejecta as a function of increasing distance from the basin rim (see their Fig. 1b). Other, larger crater to basin-like structures can be identified in the synoptic kilometer-scale roughness data. For example, the presence of the pre-Orientale Mendel-Rydberg basin can be seen in the area south of Orientale in the kilometer-scale roughness maps (Fig. 5). Furthermore, several large pre-Orientale basin circular structures in the very large crater to peak-ring basin size range suspected on the basis of topography (Head et al., in preparation, 2013) can be seen more prominently in the longer wavelength topography (Fig. 1, top). In the area just southwest of the basin, a circular feature in excess of 200 km is partly cut by, but has caused disruption of the continuity of both the Cordillera and part of the Outer Rook Rings (Fig. 5). Just northwest of the Cordillera Ring are two additional large pre-Orientale structures (Fig. 5).

The large young impact craters are rough in the kilometer-scale roughness maps, but the contrast between them and typical high-